Simultaneous electronphoton excitation of helium in a CO2 laser field

K M Dunseath, M Terao-Dunseath

Simultaneous electron-photon excitation of helium in a CO_2 laser field

K M Dunseath, M Terao-Dunseath

Institut de Physique de Rennes, CNRS-UMR 6251, Université de Rennes 1, Campus de Beaulieu, 35042 Rennes Cedex, France

Abstract. The R-matrix Floquet method is used to study electron-impact excitation of helium in the presence of a CO_2 laser field, for collision energies between 19 and 21.5 eV and laser intensities of 10^7 and 10^8 W cm^{-2}. Collision geometries with the electron incident at various angles to the laser polarization axis are considered. The signal for production of metastable states is in good agreement with the results of a low-frequency approximation and a semi-classical approach, while agreement with experiment is reasonable.

PACS numbers: 34.80.Bm, 34.80.Dp, 34.80.Kw, 34.80.Qb

Submitted to: *J. Phys. B: At. Mol. Phys.*

1. Introduction

Most studies of low-energy laser-assisted electron-atom scattering have concentrated on free-free transitions, in which the target remains in its initial state after the collision (see for example [1–5] and references therein, as well as the reviews [6, 7]). The target simply plays the role of a third body whose presence allows the electron in the field to absorb or emit photons. A more interesting process, simultaneous electron-photon excitation (SEPE), occurs when collisional and radiative interactions are strong enough to concurrently modify the internal state of the target. This can occur even when the kinetic energy E_i of the incident electron is below the field-free excitation threshold, via the absorption of photons. The kinetic energy E_f of the scattered electron is related to E_i by $E_\mathrm{f} = E_\mathrm{i} - \Delta\epsilon + N_\gamma\omega$, where $\Delta\epsilon$ is the excitation energy of the target and N_γ is the net number of photons exchanged: $N_\gamma > 0$ corresponds to absorption, $N_\gamma < 0$ to emission.

The first experimental observation of a SEPE process involving one-photon absorption was made by Mason and Newell [8, 9] for electron-helium scattering close to the $1s2s\,^3S$ threshold in a low-intensity (of the order of 10^4 $\mathrm{W\,cm^{-2}}$) CO_2 laser field (wavelength $10.6\,\mu$m, photon energy 0.117 eV) whose polarization was slightly elliptical. They also considered the SEPE process in a circularly polarized field [10]. Their experiments used time-of-flight spectroscopy to measure the difference in the production of metastable helium atoms with the laser on and with the laser off. This is expected to give a signal two to three orders of magnitude larger than that for energy-loss spectroscopy of an electron scattered through any particular angle, and hence a better signal-to-noise ratio. Wallbank *et al* [11] observed a SEPE signal with absorption of up to four photons in the same system, but with a linearly polarized CO_2 laser generating intensities of the order of 10^8 $\mathrm{W\,cm^{-2}}$. Once again, the experiment measured the difference in metastable production with the laser on and off. Wallbank *et al* extended this work to a broader energy range (up to three photon energies above the $1s2s\,^1S$ threshold) as well as to neon and argon targets [12]. While at low collision energies metastable production is exclusively via direct excitation to the $He(1s2s\,^3S)$ metastable state, at the higher collision energies considered in this last experiment the signal for metastable production also includes direct excitation into the $He(1s2s\,^1S)$ state as well as cascade from the 1s2p states. In another experiment, Wallbank *et al* considered the effect of rotating the polarization axis with respect to the incident electron beam [13]. They have also performed the only experiment using energy-loss spectroscopy, but at the much higher collision energy of 45 eV [14]. Luan *et al* [15] have considered the same scattering system at similar collision energies, but in the presence of a Nd:YAG laser field, whose wavelength is ten times smaller than that for a CO_2 laser. The intensity was 10^{10} $\mathrm{W\,cm^{-2}}$ and the polarization axis was at 45° to the incident electron beam. The SEPE signal was again measured by time-of-flight spectroscopy of the metastable atoms. A large maximum was observed at about 19.4 eV, close to the well-known $He^-(1s2s^2\,^2S)$ resonance. A detailed review of experimental work has been given by Mason [6].

Relatively few theoretical studies of the SEPE process have been performed. Early work [16, 17] was based on perturbation theory, did not include exchange and was limited to relatively high collision energies. Excitation of the helium ground state into the 1s2s ^{3}S metastable state, however, necessarily involves exchange between the scattered electron and the target. Other approaches were based on extensions to the low-frequency approximation [18–22], or an averaging of the field-free cross sections over the classical energy of the electron in the laser field [23]. These methods relate the cross section for laser-assisted scattering to those for field-free scattering in a relatively simple way. In contrast, R-matrix Floquet theory [24–26] provides a rigorous approach to laser-assisted electron scattering by a general atomic target. In addition to free-free scattering [3,4,27,28], the method has been applied in a preliminary study of the SEPE process for electron-helium scattering in a Nd:YAG laser field, where the dominant influence of the $He^-(1s2s^2\ ^2S)$ resonance was demonstrated [29], as well as to excitation in a CO_2 laser field in connection with the feasibility of observing selection rules when the laser polarization axis is perpendicular to the scattering plane [30]. In this paper, we apply the theory to the study of the SEPE process for helium in the presence of a linearly polarized CO_2 laser field at scattering energies close to the lowest field-free excitation thresholds, for laser intensities between 10^7 and 10^8 W cm^{-2}. We compare the results in particular with the experiments by Wallbank *et al* [12] covering an energy range from three photon energies below the 1s2s ^{3}S threshold to three photon energies above the 1s2s ^{1}S threshold, as well as the study of the effect of rotating the laser polarization axis relative to the incident electron beam [13].

Atomic units are used unless otherwise stated.

2. Method and computational details

R-matrix Floquet theory [24–26] provides a unified, *ab initio* and non-perturbative treatment of multiphoton ionization of complex atomic systems and of electron-atom scattering in an intense, linearly polarized, spatially homogeneous, monomode laser field. It is applicable when the laser pulse duration is much longer than that for the atomic process under study. In the dipole approximation, the laser field is described by the vector potential $\boldsymbol{A}(t) = \hat{\boldsymbol{z}}\, A_0 \cos\omega t$, where ω is the angular frequency and where the z-axis is chosen parallel to the direction of polarization. Since this time-dependent potential is periodic, the solutions $\Psi(\boldsymbol{X}, t)$ of the Schrödinger equation for the atomic system in the laser field can be expressed in terms of a Floquet-Fourier expansion:

$$\Psi(\boldsymbol{X}, t) = \mathrm{e}^{-\mathrm{i}Et} \sum_{n=-\infty}^{\infty} \mathrm{e}^{-\mathrm{i}n\omega t} \Psi_n(\boldsymbol{X}), \tag{1}$$

where $\boldsymbol{X}$ represents the set of space and spin coordinates of all the electrons, and E is the quasi-energy of the solution. Substituting this expansion into the time-dependent Schrödinger equation yields an infinite set of coupled equations for the Floquet components $\Psi_n(\boldsymbol{X})$. These are solved by adopting the standard R-matrix

approach of partitioning configuration space into two regions. In the inner region, which encompasses the charge distribution of all target states retained in the calculation, the interaction of the laser field with all $N+1$ electrons is described in the length gauge, while electron exchange and correlation are included by expanding the wave function in terms of a discrete set of antisymmetrized R-matrix basis functions. These are formed by coupling N-electron target state wave functions to a set of continuum orbitals representing the remaining electron. The Floquet Hamiltonian is diagonalized in this basis, and the resulting eigenvalues and eigenvectors used to construct the R-matrix (the inverse of the logarithmic derivative matrix) at the boundary of the inner region. The diagonalization is independent of the collision energy and is performed once for each set of good quantum numbers: these include the total magnetic number $\mathcal{M}_\mathcal{L}$, the total laser-atom parity Π and, since we neglect relativistic corrections, the total spin $\mathcal{S}$ and its projection $\mathcal{M}_\mathcal{S}$. The total angular momentum $\mathcal{L}$ of the system is no longer well-defined since the laser polarization axis introduces a preferred direction in space, breaking the spherical symmetry of the system.

In the outer region, one electron moves far from the origin so that exchange with the inner electrons can be neglected. The interaction of the field with the bound electrons is still described in the length gauge while the interaction with the continuum electron is described in the velocity gauge. For each collision energy and each set of good quantum numbers, the R-matrix on the boundary of the inner region is constructed and then transformed into a representation built from a set of field-dressed target states. Its inverse, the logarithmic derivative matrix, is propagated out to some large distance, where it is used to match the wave function to the asymptotic solutions satisfying the appropriate boundary conditions. These are defined in the acceleration frame, where the laser-electron interaction becomes vanishingly small and the equations are asymptotically uncoupled, and then transformed into the velocity gauge where they give the starting values for an asymptotic expansion. Matching to solutions satisfying scattering boundary conditions yields the reactance matrix $\boldsymbol{K}$, from which cross sections for transitions between the field-dressed target states can be calculated [26].

The field-dressed target state i is characterized by the orbital magnetic quantum number M_i, the parity π_i, spin S_i and spin magnetic quantum number M_{S_i}. As for the full scattering system, the orbital angular momentum L_i of the target is not a good quantum number. For the low-frequency laser considered here, however, there is very little dynamic Stark mixing: each field-dressed state has one dominant component of a particular orbital angular momentum, which can be used to label the state. We may therefore refer to excitation into, for example, the $1s2p\,{}^3P^o$ state, but must also specify the value of M_i.

2.1. Choice of field-free target states

The first step in any R-matrix Floquet calculation is the choice of field-free target states. In the work reported here, we employ a set consisting of the eleven lowest

Table 1. Energies and excitation thresholds for the eleven lowest states of helium. The theoretical values are compared with the accurate, non-relativistic energies taken from chapter 11 of [32] and the thresholds recommended by the National Institute of Standards and Technology (NIST) [33].

	Present (au)	Accurate (au)	Present (eV)	NIST (eV)
$1s^2$ 1^1S	−2.89877	−2.90372	0.0	0.0
1s2s 2^3S	−2.17500	−2.17523	19.695	19.820
1s2s 2^1S	−2.14557	−2.14597	20.496	20.616
1s2p 2^3P^o	−2.13246	−2.13316	20.853	20.964
1s2p 2^1P^o	−2.12270	−2.12384	21.118	21.218
1s3s 3^3S	−2.06862	−2.06869	22.590	22.719
1s3s 3^1S	−2.06061	−2.06127	22.808	22.920
1s3p 3^3P^o	−2.05787	−2.05808	22.882	23.007
1s3d 3^3D	−2.05560	−2.05564	22.944	23.074
1s3d 3^1D	−2.05558	−2.05562	22.945	23.074
1s3p 3^1P^o	−2.05452	−2.05515	22.974	23.087

states of helium, obtained by optimizing energies and oscillator strengths using the atomic structure package `CIV3` [31]. The corresponding wave functions have been used in a recent study of free-free electron-helium scattering in a CO_2 laser field [4]. The wave functions are constructed from a set of twelve orbitals: 1s, 2s, 2p, 3s, 3p, 3d, $\bar{4}$s, $\bar{4}$p, $\bar{4}$d, $\bar{4}$f, $\bar{5}$s, $\bar{5}$p, where the bar denotes a pseudo-orbital. The target state energies are presented in table 1, where they are compared with the most accurate values available [32]. We note in passing that the energies presented in columns 3-5 of table 2 in reference [4] are incorrect, and should be replaced by the values given here. The excitation thresholds are also compared to the values recommended by the National Institute of Standards and Technology (NIST) [33]. The present excitation thresholds are slightly too low, mainly due to the error in the ground state energy. A further assessment of the quality of the target state wave functions is provided by the dipole oscillator strengths and transition rates, presented in table 2 for allowed transitions involving the lowest five target states. The agreement is generally good, with the exception of the 1s2p $^1P^o \rightarrow$ 1s2s ^1S transition where the velocity form of the oscillator strength differs by almost 20% from the length form and the value given by NIST.

2.2. Field-free scattering

It is of course important to verify that the target wave functions lead to reliable cross sections for field-free scattering, in particular for excitation into all the states of helium contributing to the metastable signal measured in the experiment. We have therefore performed a standard R-matrix calculation using the states presented above. The size of the R-matrix inner region was taken to be $40\,a_0$, while total angular momenta up to $\mathcal{L} = 8$ were included, with 20 continuum orbitals per angular momentum of the incident

Table 2. Oscillator strengths f and rates A in length (L) and velocity (V) forms for dipole allowed transitions involving the five lowest states of helium, compared with the values recommended by NIST [33]. The figures in parentheses are the powers of ten by which the preceeding number should be multiplied.

Transitions		f		A ($\sec^{-1}$)	
		Present	NIST	Present	NIST
1s2p ^{1}P^o $\rightarrow$ 1s^2 ^{1}S	L	0.2836	0.2763	0.1830 (10)	0.1799 (10)
	V	0.2813		0.1814 (10)	
1s2p ^{1}P^o $\rightarrow$ 1s2s ^{1}S	L	0.3843	0.3765	0.2153 (7)	0.1975 (7)
	V	0.3282		0.1839 (7)	
1s2p ^{3}P^o $\rightarrow$ 1s2s ^{3}S	L	0.5474	0.5392	0.1061 (8)	0.1022 (8)
	V	0.5282		0.1024 (8)	

electron. In figure 1, we present the cumulated cross section for production of helium in the 1s2s ^{3}S and 1s2s ^{1}S states near the He(1s2ℓ) thresholds. In figure 1(a), we compare our results with those of a previous 5-state R-matrix calculation [29, 30], as well as a calculation based on the R-matrix with pseudostates approach (RMPS) [34], which uses a more extensive set of orbitals and pseudo-orbitals to represent the target as well as the collisional system. Increasing the size of the basis not only improves the values for the excitation thresholds (mainly by lowering the ground state energy), it also affects the magnitude of the cross sections even at the low collision energies considered here by influencing the distribution of flux amongst the elastic and inelastic channels. The first peak in the present results is about 4% smaller than that in the 5-state results, and is around 7% larger than that in the RMPS results. Beyond the 1s2p ^{3}P^o threshold, the present results and those of the RMPS calculation are in very good agreement, and are about 10% smaller than those of the 5-state calculation.

In figure 1(b), we compare the cross sections for the production of metastable helium obtained from our 11-state R-matrix calculation with those of experiment [9]. The experimental data are not absolute, but by normalizing them at the first peak they were found to be in good agreement with the results of an earlier 11-state R-matrix calculation [35] for energies up to 21 eV. The energies of the target states used in [35] are less accurate than those of the present 11-state calculation, but were adjusted to the observed values. While such shifts are relatively small compared to the state energies, they can be larger than the photon energy for a CO_2 laser, and we have not therefore made similar adjustments in our calculations. Our results are roughly 10% lower than those of [35] and in better agreement with those of the RMPS calculation. Above 21 eV, the discrepancy between the experimental data and those of [35] was attributed to excitation into the 1s2p ^{3}P^o state whose lifetime is of the order of 100 ns and which therefore decays rapidly to the 1s2s ^{3}S state. When this contribution is taken into account, however, the results of [35] overestimate those of the experiment by about 20%.

To facilitate the comparison of the shape of the results, we also show in figure 1(b)

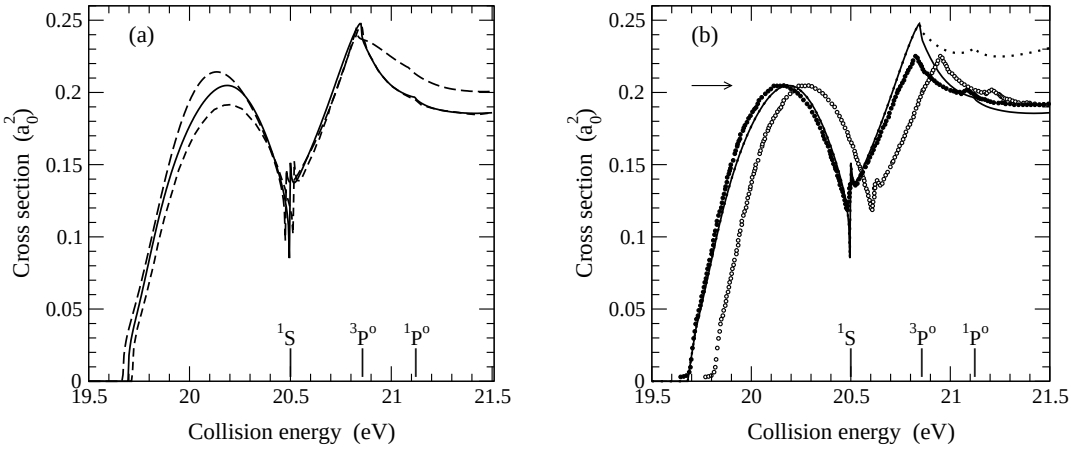

Figure 1. Cross sections for production of metastable helium in the absence of a laser field: (a) Comparison of theoretical results for the sum of excitation cross sections into the 1s2s ^{1,3}S states. Theory: ——, 11-state R-matrix calculation; – – –, 5-state R-matrix calculation [29]; - - - -, R-matrix with pseudostates calculation [34]. (b) Comparison of the results obtained with the 11-state R-matrix calculation and those of experiment [9]. Theory: ——, sum of excitation cross sections into the 1s2s ^{1,3}S states; ·····, sum of excitation cross sections into the 1s2s ^{1,3}S and 1s2p ^{3}P^o states. Experiment: ○ , normalized to the first peak in the theoretical results; ● , normalized and shifted to agree with our theoretical ^{3}S threshold.

the experimental values normalized as before and shifted so that the 1s2s ^{3}S threshold coincides with that of our 11-state R-matrix calculation. The agreement is satisfactory up to about 20.7 eV, but for higher energies the theoretical results are slightly larger than those of the experiment; in particular, the peak associated with the ^{3}P^o threshold is about 10% larger. Beyond this threshold, the 11-state results decrease rapidly, so that above the ^{1}P^o threshold they underestimate slightly the normalized experimental values. When the cascade from 1s2p ^{3}P^o state is included, the theoretical results are up to 20% larger than those of the experiment, and do not decrease as quickly with increasing energy. Further study, both experimental and theoretical, would be necessary to determine the absolute value of the cross section for production of metastable states just above the 1s2p ^{3}P^o threshold. For our purpose here, however, we may consider our field-free basis as sufficiently accurate, since the main structures in the measured SEPE signal appear below the ^{3}P^o threshold.

2.3. Laser-assisted scattering

The parameters used in the R-matrix Floquet calculations for scattering in the laser field are the same as those used above for field-free scattering. In addition, we retain 13 components in the Floquet expansion (1), from $n = -6$ to $n = 6$. For scattering geometries in which the electron is not incident parallel to the laser polarization axis, we include all contributions with $|\mathcal{M}_\mathcal{L}| \leq 5$. In the largest case, $\mathcal{M}_\mathcal{L} = 0$, the calculations for eleven field-free states involve 351 field-dressed target states coupled with

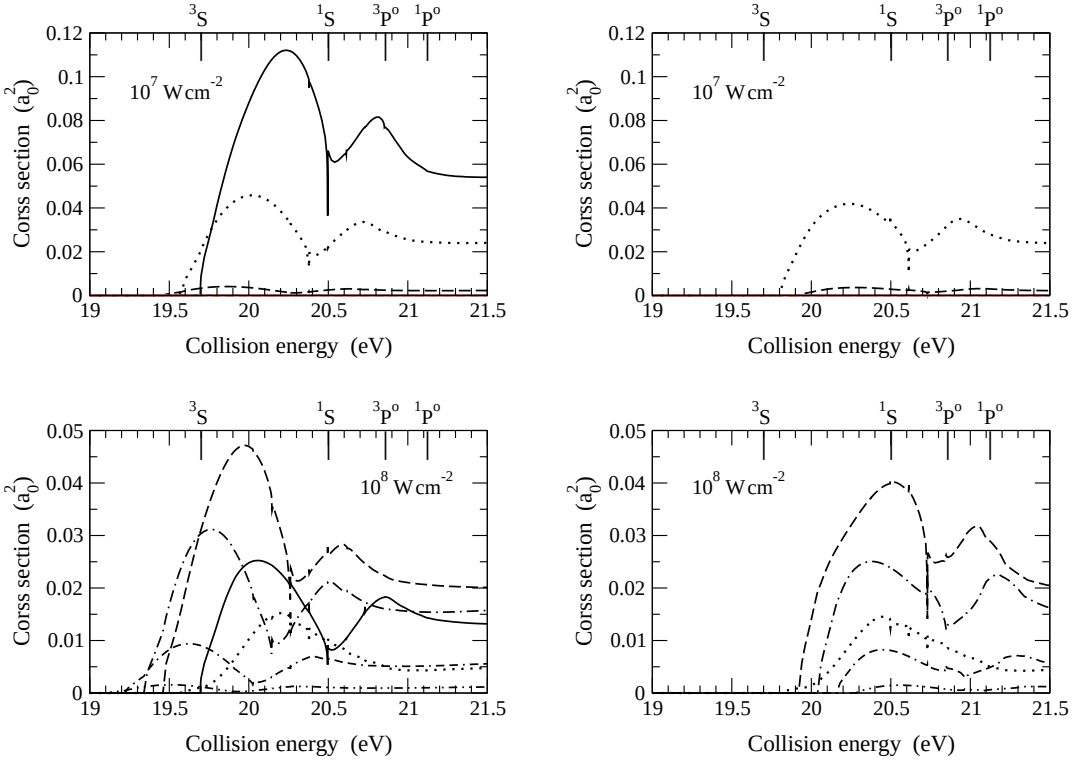

Figure 2. Cross sections for simultaneous electron-photon excitation of the 1s2s ^{3}S state of helium for laser intensities of 10^7 and 10^8 W cm^{-2}. The electron is incident parallel to the laser polarization axis. The cross sections on the left are for no net exchange of photons (——), excitation with absorption of 1 photon (· · · · · ·), excitation with absorption of 2 photons (– – –), excitation with absorption of 3 photons (– · –), excitation with absorption of 4 photons (– – · – –), excitation with absorption of 5 photons (– ·· –). The cross sections on the right are for the corresponding emission processes.

the collisional electron to give 2329 field-dressed channels. The logarithmic derivative matrix is propagated out to 200 a_0 before matching with the asymptotic expansion.

All these parameters have been tested to ensure that the results presented in the next section have converged to at least three significant figures.

3. Results and discussion

3.1. Electron incident parallel to the laser polarization axis

We first consider the scattering geometry in which the electron is incident parallel to the laser polarization axis. In figure 2, we present cross sections for simultaneous electron-photon excitation of the ground state into the 1s2s ^{3}S state with absorption or emission of up to five photons, for laser intensities of 10^7 and 10^8 W cm^{-2}. At the lower laser intensity, the cross section for excitation with no net exchange of photons dominates, being 2 to 3 times larger than those for excitation with net exchange of one photon. For

the latter, the cross section for absorption rises slightly higher than that for emission, but the shapes are generally similar. The cross sections with exchange of two photons are small and those with exchange of more than two photons are negligible.

At the higher intensity, the cross section with no net exchange of photons is reduced by approximately a factor 5 compared to its value at the lower intensity. The dominant processes are now those with net exchange of two or three photons, although the order of magnitude of the cross sections is quite small. Once again, the peak in the absorption cross section is larger than the corresponding peak in the emission cross section for the same number of photons. The cross sections for exchange of four photons are slightly smaller than those for exchange of one photon, while exchange of five photons is almost negligible.

We note that the well-known $1s2s^2\,{}^2S$ resonance, which in the field-free elastic cross section is found at approximately 0.44 eV below the $1s2s\,{}^3S$ threshold, is not visible in any of the laser-assisted cross sections presented here. This is in contrast with the SEPE process in a Nd:YAG laser [29], where the resonance is a dominant feature. It arises when the difference between the collision energy and the resonance position is an integer multiple n of the photon energy: the electron can absorb or emit n photons and be captured temporarily in the resonance. For a Nd:YAG laser, an electron incident with kinetic energy equal to the resonance energy needs to absorb only one photon in order to excite the target, while for a CO_2 laser at least four photons must be exchanged: populating the resonance and exciting the target is therefore less likely.

The cross sections for excitation into the $1s2s\,{}^3S$, ${}^1S$ and $1s2p\,{}^3P^o(M_f = 0, \pm 1)$ states, summed over the net number of photons exchanged, are presented in figure 3. Since the two and three photon exchange processes dominate at 10^8 W cm^{-2}, the main effect of increasing the laser intensity is to reduce and broaden the cross sections towards lower collision energies. The minimum between the two peaks in the ${}^3S$ excitation cross section is also mostly filled in. The cross sections are relatively unchanged near the highest collision energies considered. The periodic nature of the SEPE excitation thresholds is particularly visible in the cross sections for excitation into the ${}^1S$ state, since the field-free cross section exhibits a sharp jump at threshold due to a well-known ${}^2S$ virtual state [36]. We also show the sum of the excitation cross sections, i.e. the cross sections for the production of metastable helium, both with and without the contribution from the ${}^3P^o$ states.

In figure 4, we present the signals for the production of the $1s2s\,{}^{1,3}S$ metastable states of helium, including cascade from the $1s2p\,{}^3P^o$ state. The signal is defined as the difference of the cross sections with the laser on and with the laser off. Positive signals thus correspond to an enhancement of the production of metastable atoms by the field, negative values to a reduction. We compare the signals calculated using the R-matrix Floquet theory with those obtained using two simple formulae which relate the cross sections in the presence of the laser field to those in its absence.

The first of these is the instantaneous collision approximation (ICA) [23]. In this, the duration of the collision is supposed much shorter than the period of the laser field:

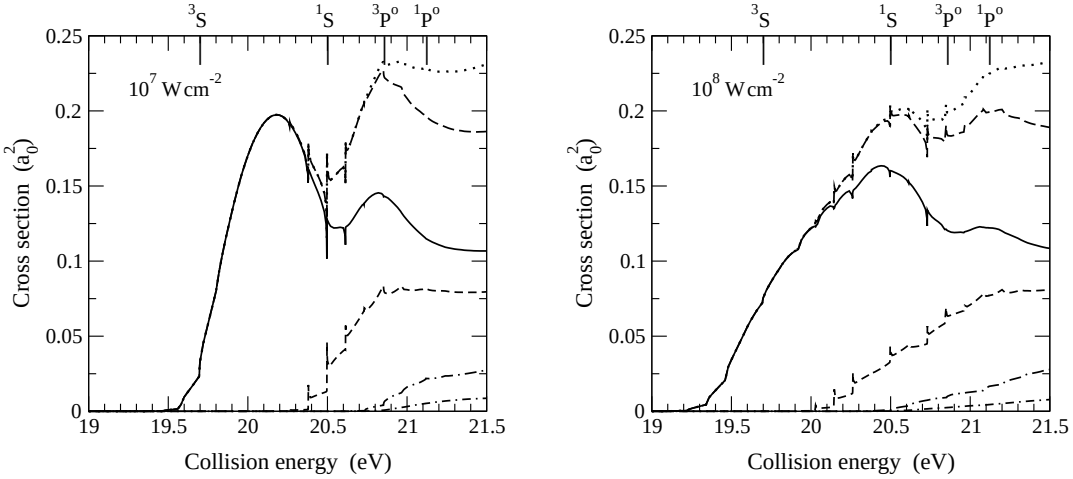

Figure 3. Cross sections for simultaneous electron-photon excitation of the 1s2s ^{3}S (——), 1s2s ^{1}S (- - - -), 1s2p ^{3}P^o($M_f = 0$) (— · —) and 1s2p ^{3}P^o($M_f = \pm 1$) (– · –) states of helium, summed over the net number of photons exchanged. Also shown are sum of the ^{3}S and ^{1}S cross sections (– – –) and the sum of the ^{3}S, ^{1}S and ^{3}P^o($M_f = 0, \pm 1$) cross sections (· · · · · ·). The electron is incident parallel to the laser polarization axis.

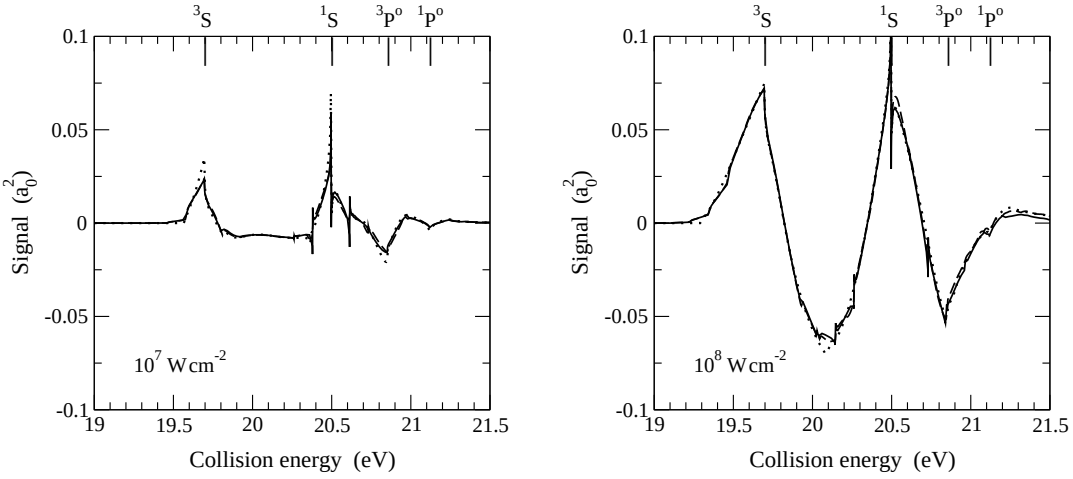

Figure 4. Comparison of theoretical SEPE signals for the production of metastable helium, including contributions from excitation into the ^{3,1}S and ^{3}P^o states: ——, R-matrix Floquet theory; · · · · · ·, instantaneous collision approximation; – – –, low-frequency approximation. The electron is incident parallel to the laser polarization axis.

in other words, the kinetic energy E_i of the incident electron must be much larger than the photon energy ω. The total cross section $\sigma^{on}(E_i)$ for a particular transition during scattering in the presence of the laser field is then obtained from the corresponding field-free cross sections σ^{off} by averaging over the electron energy oscillations in the laser field

(or equivalently over the phase ϕ of the field at the instant of collision):

$$\sigma^{\rm on}(E_{\rm i}) = \frac{1}{\pi}\int_{-\pi/2}^{\pi/2} \sigma^{\rm off}\left(E_{\rm i}^{c}(\phi)\right) {\rm d}\phi, \tag{2}$$

where $E_{\rm i}^{c}(\phi) = (\boldsymbol{k}_{\rm i} + \hat{\boldsymbol{z}}\mathcal{E}_0/\omega\,\sin\phi)^2/2$ is the classical energy of the electron in the electric field of amplitude $\mathcal{E}_0 = \omega A_0/c$. For excitation to take place, the condition $E_{\rm i}^{c}(\phi) \geq \Delta\epsilon$ must be satisfied, where $\Delta\epsilon$ is the excitation energy of the target for the transition being considered.

The second simple formula is a generalization to inelastic scattering of the well-known Kroll-Watson low-frequency approximation for free-free scattering in a laser field [20]. In this generalized low-frequency approximation (LFA), the differential cross section ${\rm d}\sigma^{\rm on}/{\rm d}\Omega$ for laser-assisted scattering summed over n, the net number of photons exchanged, is related to the field-free differential cross section ${\rm d}\sigma^{\rm off}/{\rm d}\Omega$ by

$$\frac{{\rm d}\sigma}{{\rm d}\Omega}^{\rm on}(E_{\rm i},\theta,\phi) = \sum_{n=n_0}^{\infty} \frac{K_{\rm in}}{K_{\rm fn}}\frac{k_{\rm fn}}{k_{\rm i}} J_n^2\left(\boldsymbol{\alpha}\cdot\Delta\boldsymbol{k}\right) \frac{{\rm d}\sigma}{{\rm d}\Omega}^{\rm off}(\boldsymbol{K}_{\rm fn},\boldsymbol{K}_{\rm in})\,. \tag{3}$$

The field-free differential cross sections are evaluated at the shifted momenta $\boldsymbol{K}_{\rm fn} = \boldsymbol{k}_{\rm fn} - \boldsymbol{\gamma}_n$ and $\boldsymbol{K}_{\rm in} = \boldsymbol{k}_{\rm i} - \boldsymbol{\gamma}_n$, where $\boldsymbol{\gamma}_n = n\omega\boldsymbol{\alpha}/(\boldsymbol{\alpha}\cdot\Delta\boldsymbol{k})$. The quantity $\boldsymbol{\alpha} = \hat{\boldsymbol{z}}\mathcal{E}_0/\omega^2$ is the oscillation or quiver vector of a free electron in the laser field, while $\Delta\boldsymbol{k} = \boldsymbol{k}_{\rm fn} - \boldsymbol{k}_{\rm i}$ is the momentum transfer. Energy conservation requires $k_{\rm fn}^2 = k_{\rm i}^2 - 2\Delta\epsilon + 2n\omega$. The momentum shifts $\boldsymbol{\gamma}_n$ are independent of the laser intensity, so that the entire intensity dependence is contained in the argument of the Bessel function. Just as for the ICA, the low-frequency approximation is expected to be valid when the collision energy is much larger than the photon energy. The derivation of the formula (3) also supposes that there are no sharp resonance structures in the T-matrix. We also note that, as in the free-free scattering formula, there exists a critical geometry, independent of the laser intensity, for which the denominator $\boldsymbol{\alpha}\cdot\Delta\boldsymbol{k}$ in the expression for the shift $\boldsymbol{\gamma}_n$ vanishes. The formula (3) is not expected to be valid in this case.

The results presented in figure 4 for both these approximations were obtained using the field-free cross sections from the 11-state R-matrix calculation described above, and include excitation to the ^{3}P$^{\rm o}$ states. The three sets of results all have peaks at the field-free ^{3}S and ^{1}S excitation thresholds, and a minimum close to the ^{3}P$^{\rm o}$ threshold. At 10^8 W cm^{-2}, there is also a deep minimum between the two peaks. Overall, the signal is much larger for the higher intensity. The LFA results are generally in very good agreement with those from the R-matrix Floquet calculation. At 10^8 W cm^{-2}, the ICA results are also in good agreement with those of the other calculations, but do not show the detailed structure due to the various excitation thresholds for the field-dressed target states. At 10^7 W cm^{-2}, however, the two peaks and the minimum tend to be more pronounced in the ICA results.

In figure 5, we compare the calculated SEPE signals with the measurements of Wallbank *et al* [12, 13], as a function of collision energy expressed in multiples of the photon energy below and above the field-free ^{3}S and ^{1}S excitation thresholds. The theoretical results include excitation into the ^{3}P$^{\rm o}$ states, and have been convoluted with

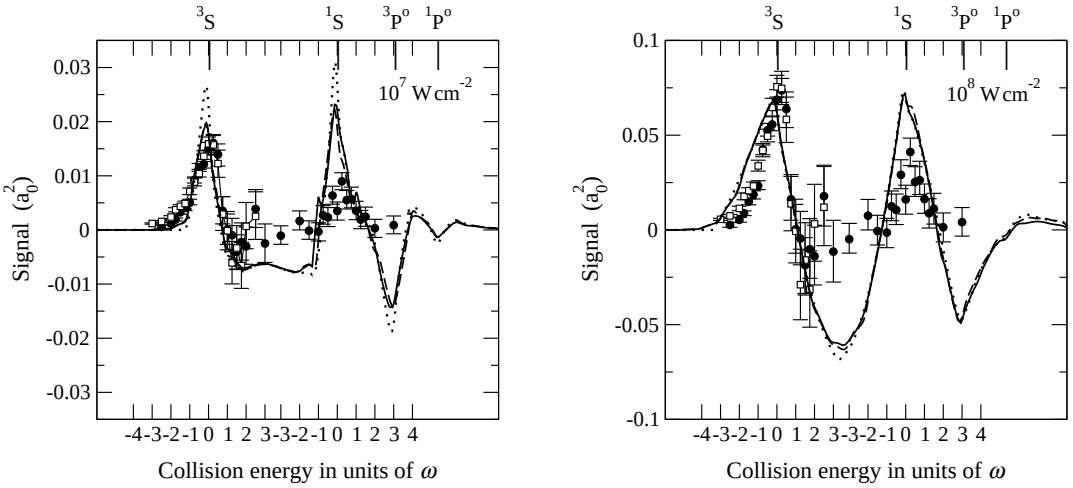

Figure 5. Comparison of the theoretical SEPE signals (including excitation into the $1s2p\,^3P^o$ states) and experiment, for an electron incident parallel to the laser polarization axis. Theory: ——, R-matrix Floquet theory; ·····, instantaneous collision approximation; – – –, low-frequency approximation. The theoretical curves have been convoluted with a gaussian of FWHM equal to 35 meV, the energy spread of the electron beam in the experiments. Experiment: ● , reference [12]; □, reference [13]. The experimental data has been normalized so as to minimize a weighted sum of the squares of the differences with the R-matrix Floquet results, see equation (4), in the energy range between -4ω and 3ω relative to the ^{3}S threshold. Hence the experimental data shown in both graphs differ only by an overall normalization factor.

a gaussian of FWHM equal to 35 meV, the energy spread of the electron beam used in the experiments. The differences between the ICA results and those of the LFA and R-matrix Floquet calculations for an intensity of 10^7 W cm^{-2} are now more clearly seen: the ICA results are almost 10% larger at the peaks near the ^{3}S and ^{1}S thresholds and almost 10% smaller at the minimum near the $^3P^o$ threshold.

The experimental results are however not on an absolute scale and must be normalized to compare with theory. One possibility is to normalize at one arbitrarily chosen energy: this may be reasonable when the curves are similar in shape, but not when they start to differ more significantly, as will be the case in some geometries considered below. Instead, we have chosen a normalization that minimizes a weighted sum of the squares of the differences with the R-matrix Floquet results,

$$\sum w \left(\sigma_{\text{theory}} - \mathcal{N}\sigma_{\text{expt}}\right)^2 \tag{4}$$

where $\mathcal{N}$ is the normalization factor to be determined and the weights w are given by $|\sigma_{\text{expt}}/\Delta\sigma|$ with $\Delta\sigma$ the relative uncertainty in the measured values. The normalization factors applied to the experimental data therefore depend on the intensity for which the calculations have been performed.

In all the theoretical curves, the second peak close to the ^{1}S threshold is slightly higher than the first peak, whereas in the experimental results it is approximately half the height of the first peak. Between the two peaks, the experimental results

remain relatively flat. At 10^7 W cm^{-2}, the theoretical signals in this region slightly underestimate the experimental values, but at 10^8 W cm^{-2} they display a deep minimum. Furthermore, the width of the first peak is better reproduced by the calculations at the lower intensity: at 10^8 W cm^{-2}, the peak in the theoretical curves is broader due to the fact that two and three photon processes are now dominant. The overall shape of the experimental results therefore appears to correspond to laser intensities of the order of a few 10^7 W cm^{-2}. Indeed, averaging over a typical intensity profile of the laser pulse as a function of time improves agreement with the experiment in the region of the first peak. In the low-frequency approximation, averaging over the temporal profile of the laser pulse corresponds to replacing the square of the Bessel function in equation (3) by

$$\frac{1}{T}\int_T J_n^2\left(\boldsymbol{\alpha}\cdot\Delta\boldsymbol{k}\right)\mathrm{d}t,$$

where T is the pulse length and where the entire time dependence of the intensity is contained in the quiver amplitude $\boldsymbol{\alpha}$ [4]. The low-frequency results presented on the left-hand side of figure 6 were obtained using the profile given by Wallbank *et al* [13], while those on the right-hand side were averaged over the profile given by Nehari *et al* [4]. The main difference between these profiles is at the peak intensity, which is twice as large in the first profile compared to the second, but which falls off more rapidly. The peak intensities in the first profile thus carry less weight in the averaging procedure. As a result, there is almost a factor two difference in the height of the first peak. In both cases, there is reasonably good agreement with the shape of the experimental results, which have been normalized to the theoretical curves using equation (4). Important differences with experiment still remain in the region between the two peaks and over the height of the second.

Close to the ^{3}P^o threshold, all three theories present a deep minimum not present in the experimental results. This minimum appears to mirror the difference in the field-free cross sections compared with experiment near the ^{3}P^o threshold, illustrated in figure 1(b). It is hence tempting to suggest that the minimum may not be physical but be due, at least in part, to inadequacies in the field-free target states used in the calculations. On the other hand, the ICA results in reference [23] also show such a minimum, even though they were obtained using the field-free experimental data of Mason and Newell [9].

3.2. Electron incident at different angles to the laser polarization axis

In the previous section, the projectile electron was incident parallel to the laser polarization axis ($\theta_\mathrm{i} = 0^o$). Here we consider geometries in which the projectile electron is incident at different angles θ_i to this axis, for the same two intensities of 10^7 W cm^{-2} and 10^8 W cm^{-2}.

In figure 7, we present the cross sections obtained using the R-matrix Floquet theory for the excitation of the 1s2s ^{3}S state, summed over the net number of photons exchanged, in an energy range of $\pm 3\omega$ about the field-free threshold. At 10^7 W cm^{-2},

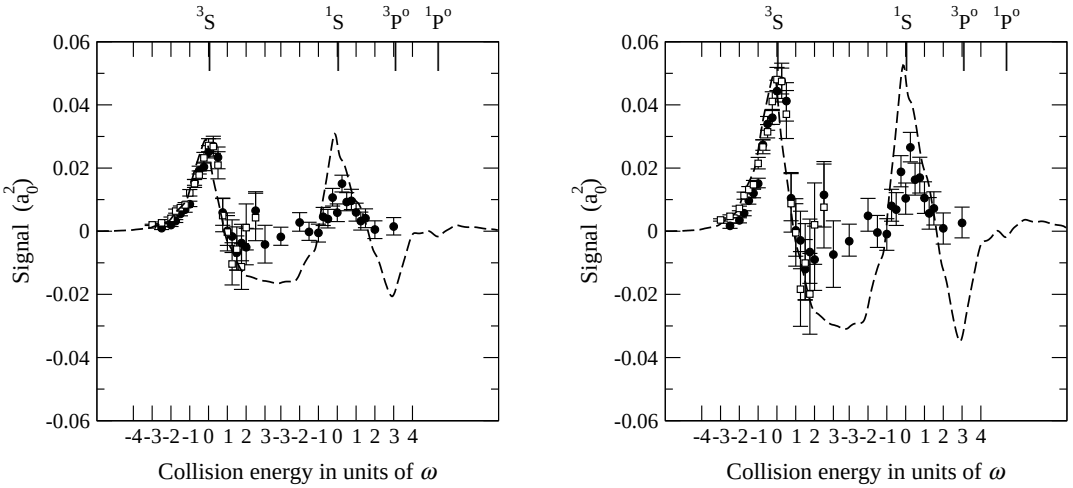

Figure 6. Comparison of the experimental signals from references [12] (●) and [13] (□) with the convoluted signal calculated using the low-frequency approximation (dashed line), including the contribution of excitation into the 1s2p ^{3}P^o states and averaged over the laser pulse profile given in references [13] (left) and [4] (right). The experimental results have been normalized to the low-frequency results at each intensity using equation (4). The electron is incident parallel to the laser polarization axis.

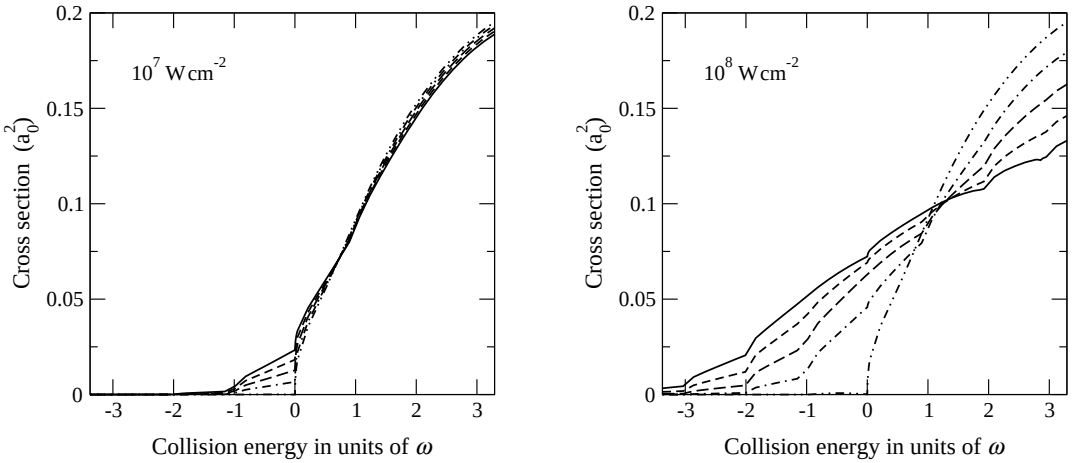

Figure 7. Cross sections for simultaneous electron-photon excitation of the 1s2s ^{3}S state of helium, calculated using the R-matrix Floquet theory and summed over the net number of photons exchanged, for an electron incident at different angles θ_i to the laser polarization axis: ——, $\theta_i = 0^o$; - - - -, $\theta_i = 30^o$; – – –, $\theta_i = 45^o$; – · –, $\theta_i = 60^o$; – ·· –, $\theta_i = 90^o$. The collision energy is in units of the photon energy, relative to the ^{3}S threshold.

the results above this threshold show little sensitivity to the value of θ_i, whereas below threshold the contributions from excitation with net absorption of one or more photons diminish with increasing θ_i. The cross sections at 10^8 W cm^{-2} are much more sensitive to the value of θ_i. As remarked earlier, for $\theta_i = 0^o$ the cross sections are dominated

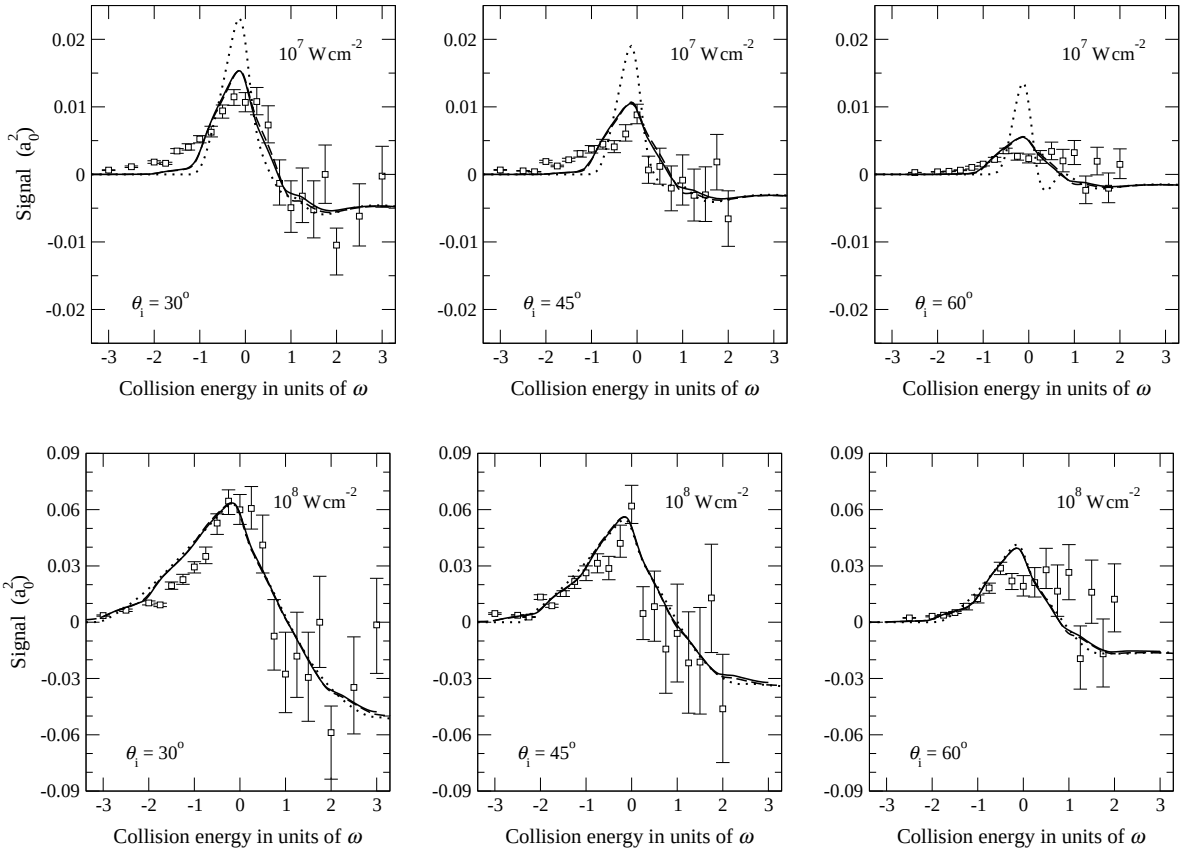

Figure 8. Comparison of the theoretical SEPE signals and experiment, for an electron incident at different angles $\theta_{\rm i}$ to the laser polarization axis. The collision energy is in units of the photon energy, relative to the ^{3}S threshold. The solid, dotted and dashed lines are respectively the results of the R-matrix Floquet theory, the instantaneous collision approximation and the low-frequency approximation. The experimental results are from reference [13], and have been normalized to the R-matrix Floquet results at each intensity using equation (4). The upper row corresponds to a laser intensity of 10^7 W cm^{-2}, the lower row to an intensity of 10^8 W cm^{-2}.

by processes involving net exchange of two or three photons. As $\theta_{\rm i}$ increases however, these processes become less important and the net exchange of fewer photons becomes dominant. As a result, the cross sections below threshold are progressively reduced while above threshold they are increased. More specifically, at $\theta_{\rm i} = 30^{\rm o}$ the dominant processes is two-photon exchange, the next is one-photon exchange; at $\theta_{\rm i} = 45^{\rm o}$ it is one-photon exchange then two-photon exchange, while at $\theta_{\rm i} = 60^{\rm o}$ it is one-photon exchange followed by no net exchange of photons. Finally, at $\theta_{\rm i} = 90^{\rm o}$, processes involving net photon exchange are almost completely suppressed. At both intensities, the cross section for no net exchange of photons is very close to that for field-free scattering, so that the resultant SEPE signal is very weak.

This behaviour is consistent with the low-frequency approximation (3). The magnitude of the cross section for exchange of n photons depends on the factor $J_n^2(x)$, with $x = \alpha(k_{{\rm f}n}\cos\theta_{\rm f} - k_{\rm i}\cos\theta_{\rm i})$. Since $k_{\rm i} >> k_{{\rm f}n}$, the second term dominates the first

and x can be quite large for small values of θ_i. As θ_i increases however, the amplitude of the second term decreases, eventually vanishing at $\theta_\mathrm{i} = 90^\mathrm{o}$. The overall value of x and hence the magnitude of the cross sections for exchange of n photons will also decrease, while that for no net exchange of photons will increase. We note however that as $\theta_\mathrm{i} \to 90^\mathrm{o}$, the momentum shift $\boldsymbol{\gamma}_n$ becomes very large, leading to problems in the numerical evaluation of the low-frequency approximation since the field-free differential cross section has to be known over a very wide range of energies.

In figure 8, we compare the theoretical signals convoluted over the energy distribution of the electron beam with those of the experiment [13], for three collision geometries in which the projectile electron is incident at an angle θ_i equal to 30^o, 45^o and 60^o to the laser polarization axis. The theoretical results have been obtained for a laser intensity of 10^7 W cm^{-2} (upper row) and 10^8 W cm^{-2} (lower row).

As before, there is very good agreement between the three sets of theoretical results at the higher intensity. The height of the peak decreases slowly with increasing θ_i, and is approximately 94%, 83% and 58% of the height at $\theta_\mathrm{i} = 0^\mathrm{o}$ for $\theta_\mathrm{i} = 30^\mathrm{o}$, 45^o and 60^o respectively. At 10^7 W cm^{-2}, the ICA results differ considerably from those of the other two methods. As in the case where $\theta_\mathrm{i} = 0^\mathrm{o}$, the ICA results show a more pronounced peak, which does not decrease as rapidly with increasing θ_i as in the R-matrix Floquet and low-frequency results. For $\theta_\mathrm{i} = 30^\mathrm{o}$, 45^o and 60^o, the height of the peak in the latter is respectively 78%, 54% and 28% of its value for $\theta_\mathrm{i} = 0^\mathrm{o}$: in the ICA results, these values are 87%, 71% and 50%. There is also a discrepancy in the width of the peak, which is narrower in the ICA results. Futhermore, at $\theta_\mathrm{i} = 60^\mathrm{o}$, a small oscillation appears in the ICA results between the threshold and one photon energy above threshold, which is not present in the other theoretical data.

At $\theta_\mathrm{i} = 30^\mathrm{o}$, the comparison with experiment is qualitatively similar to $\theta_\mathrm{i} = 0^\mathrm{o}$: at the lower intensity the peak in the theoretical results is slightly narrower than that in the experimental values, while at the higher intensity it is slightly broader. At $\theta_\mathrm{i} = 45^\mathrm{o}$ however, the results at the higher intensity agree quite well with the experiment, especially at lower energies where the error bars are small. At $\theta_\mathrm{i} = 60^\mathrm{o}$, there is also good agreement at the higher intensity up to about one half the photon energy below threshold. Beyond this, there appears to be a small structure in the experimental results at threshold that is not present in the averaged theoretical signals. It should be noted that there is considerable scatter in the experimental results above threshold, with a number of points now positive, while the theory remains slightly negative. The experimental error bars are however much larger above threshold than below.

As θ_i increases, the height of the peak in the measurements of the metastable yield (the raw, un-normalized data) decreases, so that at $\theta_\mathrm{i} = 30^\mathrm{o}$, 45^o and 60^o, it is approximately 63%, 51% and 27% of its value for $\theta_\mathrm{i} = 0^\mathrm{o}$. These values are somewhat lower than those for the R-matrix Floquet calculation at 10^8 W cm^{-2}, but they are similar to the theoretical results at 10^7 W cm^{-2} for the latter two angles.

Finally, for completeness, in figure 9 we compare the experimental results for $\theta_\mathrm{i} = 90^\mathrm{o}$, normalized as before, with the theoretical values calculated at an intensity

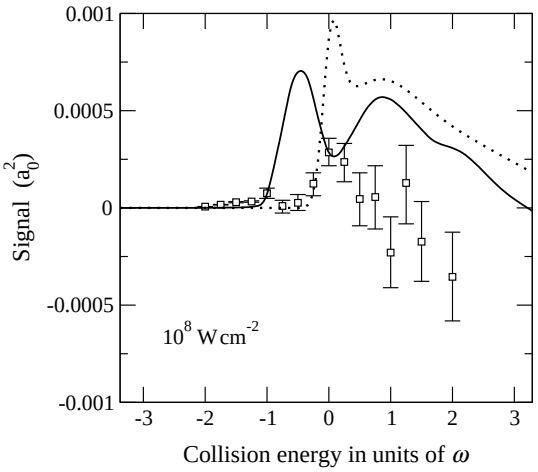

Figure 9. Comparison of experimental SEPE signals for an electron incident at an angle $\theta_i = 90^o$ to the laser polarization axis with those obtained using R-matrix Floquet theory and the instantaneous collision approximation, computed for an intensity of 10^8 W cm^{-2}. The solid and dotted lines are respectively the results of the R-matrix Floquet theory and the instantaneous collision approximation. The experimental results are from reference [13], and have been normalized to the R-matrix Floquet results folliwing equation (4). The collision energy is in units of the photon energy, relative to the ^{3}S threshold.

of 10^8 W cm^{-2}. The results at 10^7 W cm^{-2} (not shown) are similar in form but are a factor ten smaller. Only the results obtained using the R-matrix Floquet theory and the instantaneous collision approximation are shown; as mentioned above, the numerical evaluation of the low-frequency approximation at this angle is not reliable due to large momentum shifts required. As expected, the signals are very weak, nearly thirty times smaller than for $\theta_i = 60^o$. On the other hand, the raw, un-normalized experimental data is surprisingly large. In their paper, Wallbank *et al* [13] stated that the height of the peak in the data for $\theta_i = 90^o$ is approximately 30% of its value for $\theta_i = 0^o$. This is much higher than the corresponding percentage for the theoretical results, which is of the order of 1%. The shapes of all three sets of results are quite different. The RMF signal has a minimum at threshold, whereas both the ICA and experimental results display a peak at this energy. While the theoretical values remain positive for longer as the collision energy increases, the experimental signal rapidly becomes negative.

4. Conclusions

R-matrix Floquet theory offers the possibility of performing *ab initio* multichannel calculations for laser-assisted scattering, including electron exchange. It can therefore be used to benchmark other simple approximations. Here we have verified the reliability of the low-frequency approximation as extended to inelastic collisions by Mittleman [20] for the case of electron-helium scattering in a CO_2 laser field. In contrast, the instantaneous

collision approximation, while working well at one higher intensity, gives slightly different results than the other theories at an intensity ten times lower. Differences with the ICA results at low intensity become more apparent when the electron is not incident parallel to the laser polarization axis.

The agreement obtained with the experimental results by Wallbank *et al* [12,13] for various collision geometries is satisfactory. The fact that the experimental results are not absolute complicates the comparison, and the quality of the agreement can depend on the normalization procedure adopted. We have shown, for instance, that averaging the theoretical results over two different intensity profiles gives good agreement with experiment in both cases, even though the magnitudes of the SEPE signals are different. This emphasizes the need for measurements on an absolute scale as well as more precise information about the intensity profile of the laser pulse. Both these ingredients are necessary if more detailed comparisons are to be made.

References

[1] N. J. Kylstra and C. J. Joachain 1999 *Phys. Rev. A* **60** 2255–2268
[2] B. Wallbank and J. K. Holmes 2001 *Can. J. Phys.* **79** 1237–1246
[3] K. M. Dunseath and M. Terao-Dunseath 2004 *J. Phys. B: At. Mol. Opt. Phys.* **37** 1305–1320
[4] D. Nehari, J. K. Holmes, K. M. Dunseath, and M. Terao-Dunseath 2010 *J. Phys. B: At. Mol. Opt. Phys.* **43** 025203
[5] B. A. deHarak, L. Ladino, K. B. MacAdam, and N. L. S. Martin 2011 *Phys. Rev. A* **83(2)** 022706
[6] N. Mason 1993 *Rep. Prog. Phys.* **56** 1275–1346
[7] F. Ehlotzky, A. Jaroń, and J. Z. Kamiński 1998 *Phys. Rep.* **297** 63–153
[8] N J Mason and W R Newell 1987 *J. Phys. B: At. Mol. Opt. Phys.* **20(10)** L323–L326
[9] N J Mason and W R Newell 1989 *J. Phys. B: At. Mol. Opt. Phys.* **22(5)** 777–96
[10] N J Mason and W R Newell 1990 *J. Phys. B: At. Mol. Opt. Phys.* **23** L179–L182
[11] B. Wallbank, J. K. Holmes, L. LeBlanc, and A. Weingartshofer 1988 *Z. Phys. D* **10** 467–472
[12] B. Wallbank, J. K. Holmes, and A. Weingartshofer 1989 *J. Phys. B: At. Mol. Opt. Phys.* **22** L615–L619
[13] B. Wallbank, J. K. Holmes, and A. Weingartshofer 1990 *J. Phys. B: At. Mol. Opt. Phys.* **23** 2997–3005
[14] B. Wallbank, J. K. Holmes, and A. Weingartshofer 1989 *Phys. Rev. A* **40(9)** 5461–5463
[15] S. Luan, R. Hippler, and H. O. Lutz 1991 *J. Phys. B: At. Mol. Opt. Phys.* **24** 3241–3249
[16] S Jetzke, F H M Faisal, R Hippler, and H O Lutz 1984 *Z. Phys. A* **315(3)** 271–276
[17] S Jetzke, J Broad, and A Maquet 1987 *J. Phys. B: At. Mol. Phys.* **20** 2887–2897
[18] S Geltman and A Maquet 1989 *J. Phys. B: At. Mol. Opt. Phys.* **22(14)** L419–L425
[19] A Maquet and J Cooper 1990 *Phys. Rev. A* **41(3)** 1724–1727
[20] M H Mittleman 1980 *Phys. Rev. A* **21(1)** 79–84
[21] M H Mittleman 1993 *J. Phys. B: At. Mol. Opt. Phys.* **26(16)** 2709–2716
[22] P D Fainstein, A Maquet, and W C Fon 1995 *J. Phys. B: At. Mol. Opt. Phys.* **28** 2723–2728
[23] B N Chichkov 1990 *J. Phys. B: At. Mol. Opt. Phys.* **23(13)** L333–L338
[24] P. G. Burke, P. Francken, and C. J. Joachain 1991 *J. Phys. B: At. Mol. Opt. Phys.* **24** 761–790
[25] M. Dörr, M. Terao-Dunseath, J. Purvis, C. J. Noble, P. G. Burke, and C. J. Joachain 1992 *J. Phys. B: At. Mol. Opt. Phys.* **25** 2809–2829
[26] M. Terao-Dunseath and K. M. Dunseath 2002 *J. Phys. B: At. Mol. Opt. Phys.* **35** 125–140
[27] D. Charlo, M. Terao-Dunseath, K. M. Dunseath, and J.-M. Launay 1998 *J. Phys. B: At. Mol. Opt. Phys.* **31** L539–L546

[28] K. M. Dunseath and M. Terao-Dunseath 2006 *Phys. Rev. A* **73** 053407–1:7
[29] M. Terao-Dunseath, K. M. Dunseath, D. Charlo, A. Hibbert, and R. J. Allan 2001 *J. Phys. B: At. Mol. Opt. Phys.* **34** L263–L270
[30] K. M. Dunseath, M. Terao-Dunseath, and G. Bourhis 2005 *Phys. Rev. A* **72** 033410–1:9
[31] A Hibbert 1975 *Comput. Phys. Commun.* **9** 141–172
[32] G. W. F. Drake, editor *Handbook of Atomic, Molecular and Optical Physics* Springer 2006
[33] Yu Ralchenko, A E Kramida, J Reader, and the NIST ASD Team NIST Atomic Spectra Database 2010
[34] K. Bartschat, E. T. Hudson, M. P. Scott, P. G. Burke, and V. M. Burke 1996 *Phys. Rev. A* **54(2)** R998–R1001
[35] K. A. Berrington, P. G. Burke, L. C. G. Freitas, and A. E. Kingston 1985 *J. Phys. B: At. Mol. Phys.* **18** 4135–4147
[36] K A Berrington, P G Burke, and A L Sinfailam 1975 *J. Phys. B: At. Mol. Phys.* **8(9)** 1459–1473